# $K^-$–$p$ Elastic Scattering in the 1-BeV/$c$ Range*

L. SODICKSON,† I. MANNELLI,‡ D. FRISCH, AND M. WAHLIG
*Department of Physics and Laboratory for Nuclear Science, Massachusetts Institute of Technology, Cambridge, Massachusetts*

(Received 23 September 1963)

Differential $K^-$–$p$ elastic-scattering cross sections have been measured at four momenta in the range corresponding to the $T=0$, 1815-MeV $K^-$–$p$ resonance, using a cylindrical spark chamber surrounding a liquid-hydrogen target. The integrated elastic-scattering cross sections follow the known resonant behavior of the total cross section, and are (18.7±0.7), (23.3±1.0), (17.3±1.1), and (15.2±0.7) mb at 820, 1040, 1150, and 1260 MeV/$c$ bombarding momentum, respectively. It is necessary to include $\cos^5\theta^*$ terms in order to fit the angular distributions at 1040 and 1150 MeV/$c$, and within the accuracy of the experiment higher terms in $\cos\theta^*$ are not needed throughout the resonance region. This implies that the resonance is due to $D_{5/2}F_{5/2}$ interference, and that the simplest assignment for the spin of the resonance is $J=5/2$. No conclusion can be inferred about the parity.

## I. INTRODUCTION

THE $K^-$–$p$ total cross section has been extensively measured up to very high incident momentum. The low-energy results from emulsion and bubble-chamber experiments[1–5] showed a strongly decreasing cross section with increasing momentum up to a few hundred MeV/$c$. Chamberlain *et al.*[6] observed a striking 15-mb resonance on a 35-mb background cross section near 1-BeV/$c$ bombarding momentum. Above 2 BeV/$c$ the total cross section so far shows no significant structure, decreasing slowly from roughly 27 mb at 2.5 BeV/$c$ to approximately 20 mb at 20 BeV/$c$.[7–10] The object of the present experiment was to measure differential elastic scattering cross sections in the region around 1 BeV/$c$ in the hope of obtaining some information about the detailed properties of the resonance there.

* This work is supported in part through AEC Contract AT(30-1)-2098, by funds provided by the U. S. Atomic Energy Commission.

† Based on a thesis submitted in partial fulfillment of the requirements for the degree of Doctor of Philosophy at Massachusetts Institute of Technology, Cambridge, Massachusetts, January 1963.

‡ NATO Fellow, on leave of absence from Pisa University, Pisa, Italy.

[1] S. C. Freden, F. C. Gilbert, and R. S. White, Phys Rev. **118**, 564 (1960).

[2] Paul Nordin, Jr., Phys. Rev. **123**, 2168 (1961).

[3] W. E. Humphrey and R. R. Ross, Phys. Rev. **127**, 1305 (1962).

[4] M. Ferro-Luzzi, R. D. Tripp, and M. B. Watson, Phys. Rev. Letters **8**, 28 (1962).

[5] P. L. Bastien and J. P. Berge, Phys. Rev. Letters **10**, 188 (1963).

[6] O. Chamberlain, K. M. Crowe, D. Keefe, L. T. Kerth, A. Lemonick, Tin Maung, and T. F. Zipf, Phys. Rev. **125**, 1696 (1962).

[7] V. Cook, B. Cork, T. F. Hoang, D. Keefe, W. A. Wenzel, and T. F. Zipf, Phys. Rev. **123**, 320 (1961).

[8] A. N. Diddens, E. W. Jenkins, T. F. Kycia, and K. F. Riley, Brookhaven National Laboratory Report BNL 6962 (to be published).

[9] G. von Dardel, D. H. Frisch, R. Mermod, R. H. Milburn, P. A. Piroue, M. Vivargent, G. Weber, and K. Winter, Phys. Rev. Letters **5**, 333 (1960).

[10] W. F. Baker, R. L. Cool, E. W. Jenkins, T. F. Kycia, R. H. Phillips, and A. L. Read, Phys. Rev. **129**, 2285 (1963).

## II. EXPERIMENTAL METHOD

### A. General Description

This experiment was performed in a secondary beam from the Brookhaven A.G.S. A cylindrical spark chamber subtending a large solid angle at the central liquid-hydrogen target was used as the detector. The good time-resolution of the spark chamber allowed the use of an unseparated beam. The selection of the $K^-$ mesons from the large background of $\pi$ and $\mu$ mesons was made electronically, using a differential Čerenkov counter after momentum analysis. The spark chamber was triggered whenever an incident $K$ meson produced at least one charged particle on each side of the beam, and did not fire a downstream veto counter. Photographs were taken of each spark-chamber discharge, and the geometry of each event subsequently reconstructed from measurements on the sparks in each photograph.

Elastic-scattering events were selected on the basis of the coplanarity of the tracks and on the closeness of the polar scattering angles to elastic kinematics. From a total of 80 000 photographs, approximately 800 elastic events inside the fiducial region were obtained at each of the bombarding momenta 820, 1040, and 1260 MeV/$c$, and 400 events at 1150 MeV/$c$.

### B. The $K^-$ Beam Setup

Figure 1 is a sketch, not to scale, of the layout of the apparatus at the A.G.S. The secondary particles produced by the primary protons in the machine target left the vacuum chamber of the A.G.S. through a 0.010-in. aluminum window. Those produced at 30° to the circulating proton beam passed through collimator 1, were deflected by 15° in the momentum analyzing magnet, and then left the A.G.S. tunnel via a channel through the shielding wall. A three-counter telescope $S_1S_2S_3$ defined the beam direction, and ensured that beam particles did not strike the walls of collimator 2. Collimator 2 and the anticoincidence counters $V_0$ and

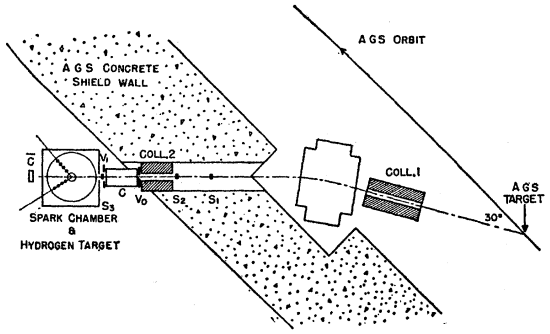


FIG. 1. A schematic drawing of the experimental setup.

$V_1$ protected the Čerenkov counter and the spark chamber from off-axis particles.

$S_1$ was 1×2 in., $S_2$ was 1.25×2 in., and $S_3$ was 1.5×2 in., all of $\frac{1}{8}$-in.-thick plastic scintillator. $S_1$ and $S_2$ were separated by 10 ft, and the distance between the center of the analyzing magnet and $S_3$ was 20 ft. Collimator 1 was made of brass, was 36 in. long, and had a 1.5-in.-wide by 0.5-in.-high channel through it. The solid angle subtended at the A.G.S. target was 30 $\mu$sr. The divergence of the beam entering the spark chamber, set by the multiple scattering in the Čerenkov counter, was approximately $\pm 0.5°$. The momentum spread accepted was $\pm 2.5\%$. The total flight path from the internal target to the spark chamber was 40 ft, corresponding to a 10% survival of charged $K$ mesons at 1 BeV/$c$.

The absolute calibration of the beam momentum and its spread were obtained mainly from a calculation based on the geometry, and on field measurements in the magnet. As a check, beam protons were separated by time-of-flight and their range measured, with the magnet set for a mean momentum of 800 MeV/$c$. The central momentum and the momentum spread of the differential momentum spectrum obtained from the range curve were in good agreement with the calculated values.

In addition, the nominal value of the beam momentum was roughly confirmed by the observed location of the $K^- - p$ resonance, as measured by the fraction of the $K^-$ mesons which interacted in the hydrogen target.

During the course of the experiment, the A.G.S. energy was varied between 15 and 30 BeV, and Be, Al, and polyethylene machine targets were used to fulfill the requirements of the primary experiments. At the spark chamber, the range of yields per machine pulse at primary energy of 30 BeV with $2\times10^{11}$ circulating protons was 15–30 Čerenkov-selected $K^-$ mesons and 5000–8000 $\pi^-$ mesons, depending on the $K$ momentum. Both the yield of $K^-$ mesons and the $K/\pi$ ratio were smaller by almost a factor of two at 15 BeV primary energy. The increased repetition rate of the A.G.S. at 15 BeV very nearly compensated for the loss of $K$ intensity, but the $\pi$ contamination was larger by the factor of two.

### C. The Spark Chamber and Trigger System

The details of the construction and the optical system of the cylindrical spark chamber have been described previously.[11] The chamber consisted of twelve closely spaced coaxial cylinders surrounding the 4-in.-diam liquid-hydrogen target, which are coaxial with the vertical cylinders. Photographs were taken along the cylinder axis from one end. Two images of each spark were produced on the film, one directly, and the other by reflection from one of fifteen 2° stereo mirrors placed at the other end. Figure 2 is a sketch of the cross section of the spark chamber, hydrogen target, and trigger counters.

At the time of this experiment, the available beam spill of the A.G.S. was short (5–20 msec) and strongly structured. A 2-in.-wide slot was left through the plates in the forward and backward directions (see Fig. 2) to allow the main beam to pass through the entire spark chamber without producing unnecessary ionization in the chamber gaps, and also to limit the number of triggers due to interactions outside the liquid hydrogen. The presence of this slot limits to greater than 10° the laboratory scattering angles which could be observed.

A 5-in.-diam Čerenkov counter 40 in. downstream from the hydrogen cell was used in anticoincidence to indicate that an entering $K$ meson had interacted or decayed within the spark-chamber assembly. A differential Čerenkov counter was used to avoid unnecessary veto signals from the $\pi$ mesons.

Roughly 2% of the incident $K$ mesons interacted in the hydrogen, while approximately 25% decayed before reaching the veto counter, primarily in the $K\mu 2$ mode which yields only one charged secondary. A coincidence trigger requiring at least two charged outgoing particles was used to eliminate this large source of unnecessary triggers. Two semicylindrical $\frac{3}{8}$-in.-thick plastic scintillators, $S_L$ and $S_R$ (shown in Fig. 2), were mounted

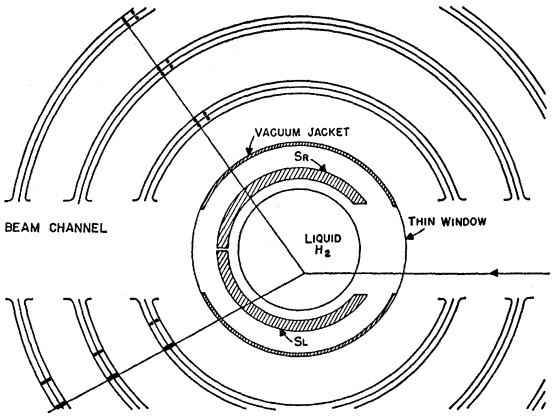


FIG. 2. A cross-sectional view of the spark chamber, hydrogen target cell, and trigger counters ($S_L$ and $S_R$).

[11] M. A. Wahlig, A. Buffington, D. H. Frisch, D. A. Hill, and L. Sodickson, Rev. Sci. Instr. 33, 539 (1962).

inside the vacuum jacket of the hydrogen target, coaxial with and closely surrounding the 4-in.-diam target cell. The beam entered the cell through a 3-in.-sq hole cut through the 6-in.-high cylinders in the upstream direction, and a coincidence between both half-cylinders was required before the chamber was triggered. This system was vulnerable to the three pion decay mode of the $K$, for which the branching ratio is 6%,[12] from a small region near the hydrogen cell. Such decays were indeed observed with a frequency comparable to that of the elastic scattering events.

### D. Čerenkov Counters

A sketch of the counter used to separate the $K$ mesons from pi mesons and antiprotons is shown in Fig. 3. This counter is similar in principle to the one used by Chamberlain *et al.*[6] in their total cross-section work. To change the selected velocity over the momentum range of this experiment, the concentration of the sugar-water solution used as the radiator was changed. The solutions used ranged in index of refraction between 1.33 and 1.45.

The Čerenkov cone angles of the $K$ and $\pi$ light differed by a few degrees in the radiator. The angular difference was greatly amplified upon refraction at the quartz-air interface because the cone angles were close to the critical angle for that surface. Indeed, for $\beta_K > 0.89$, the $\pi$ light cone angle was larger than the critical angle, so that the light was totally internally reflected and absorbed by the blackened inside walls of the radiator container.

Light leaving the quartz in the angular range of $60 \pm 3°$ with respect to the beam axis was brought to a ring focus by a cylindrically symmetric mirror of circular cross section which was made of carefully polished aluminum. The mirror was made by turning the

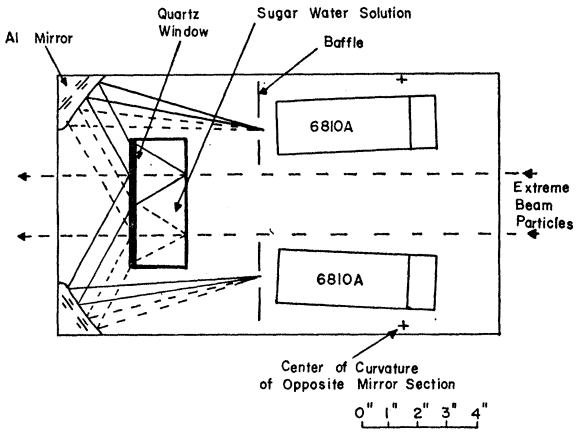


FIG. 3. A sketch of the Čerenkov counter used to separate $K$ and $\pi$ mesons at 1 BeV/$c$.

[12] M. Gell-Mann and A. H. Rosenfeld, Ann. Rev. Nucl. Sci. 7, 457 (1957).

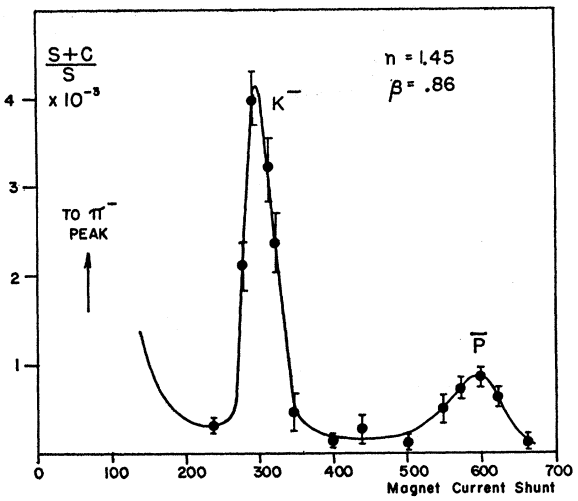


FIG. 4. A response curve for the Čerenkov counter. The pion contamination in the selected $K$ beam was estimated from the ratio of the $K$ peak to the $K$-$\pi$ valley. For this curve, it was approximately 7%. The peak-to-valley ratio was frequently monitored during the experimental runs, where it ranged between 1.6 and 4%, depending on the momentum.

9.5-in.-diam blank in a lathe, and swinging the cutting tool on a 13-in.-diam circle with its center offset by 4.25 in.

After the ring focus some additional light-gathering was provided by shaped aluminized styrene mirrors. The active region of the radiator in a 2-in.-diam cylinder about the central axis. The counter was 2 in. thick. Four 6810A photomultipliers were used to view the focal ring, with a coincidence between all four required to give a Čerenkov output pulse. The entire counter fits within a box with dimensions $10 \times 10 \times 20$ in., designed to fit inside the 12- × 12-in. channel through the A.G.S. shielding wall.

Figure 4 shows a response curve, taken by varying the current in the analyzing magnet. The ordinate is the ratio of the beam telescope plus Čerenkov counter coincidences to the telescope counts alone. The large peak in the figure is due to $K$ mesons, and the smaller one to antiprotons.

Peak efficiencies of 40–70% were typical. The four-fold coincidence requirement was stringent enough so that the efficiency for counting pi mesons when tuned for $K$ mesons was of the order of $2 \times 10^{-5}$. It was not necessary to anti on the $\pi$ light to achieve this rejection.

The angular acceptance was chosen to give good response over a $\pm 6\%$ momentum slice for $K$ mesons at 1 BeV/$c$, roughly twice the momentum spread desired for the experiment. With the momentum spectrum of the beam unfolded, the resolution curves for this Čerenkov counter have a half-width in $\beta$ of 0.025.

An estimate of the pion contamination of the data was obtained by extrapolation of the background counting ratio between the pi and $K$ peaks under the

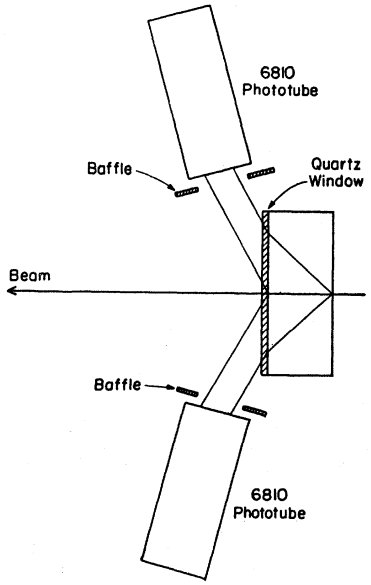


FIG. 5. A sketch of the Čerenkov counter used for the downstream anti.

$K$ peak. This was typically 1.6–4% during the data runs, and was monitored frequently.

Figure 5 shows the design of another Čerenkov counter, used for the downstream anti. Its angular acceptance was twice as large as that of the focusing counter described above, and the resolution curve was correspondingly broader. For use in anticoincidence, an output pulse in any of the four phototubes produced a veto pulse. Operated in this way, this counter was found to give a veto pulse for 98% of the particles with $0.84 \lesssim \beta \lesssim 0.94$ over its full 5-in. diameter, and to give a veto pulse for only 10% of the pions with $\beta > 0.99$.

## III. DATA ANALYSIS

### A. General Description

In order to select candidates for elastic scattering events, all of the photographs were double scanned for two-pronged events. Most of the selected events were measured only once. The volume of the parallelepiped with one of its unit edges along the telescope-defined incident beam direction and the others along the two outgoing tracks was used as a measure of the coplanarity of the event. The polar scattering angles and their errors were used to fit the event to elastic kinematics, and to estimate the probability that each event was an elastic one. A fiducial region was selected through which the detection efficiency was reasonably uniform. Each observed event was assigned a weight which included the corrections for its detection efficiency and for the decay and interaction of the scattered meson and recoil proton. The coplanar elastic events originating in the fiducial volume were divided into bins in $\cos\theta^*$, where $\theta^*$ is the center-of-mass scattering angle, and counted according to their weights.

### B. Analysis Procedure

The pictures were measured on Recordak model MPC-1 film readers, which have rotatable projection heads. The amount of rotation of a head could be read from an accurate angular scale which we had scribed on it. The projected angles of tracks relative to the fiducial marks defining the incoming beam direction were measured by rotating the head until the chosen track lay parallel to the screen axis. The point of interaction was reconstructed by extrapolation back along the two outgoing tracks with rulers, and its film-plane coordinates read from a fiducial gridwork included in the center of each picture. The dip angles and height of the event were obtained from measurements of the separation between the two images of each spark on a gridwork fixed in the viewing plane of the projector.

### C. Scanning and Measurement Errors and Fiducial Region

The efficiency of the double scan was estimated as approximately 97% by a comparison of its results with a sample of 10% of the data which were scanned a third time and roughly measured by two of the authors. This sample was at an incident momentum of 1040 MeV/$c$, where there were many backscattering events, for which the scanning efficiency was expected to be lowest.

The errors inherent in the measurements were estimated by a comparison of several independent measurements of the same events by different scanners using different scanning machines. A sample of approximately 150 doubly measured events was used. The

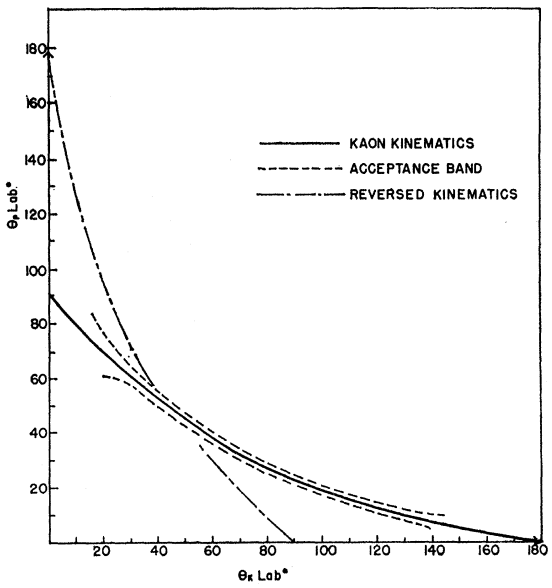


FIG. 6. A plot of the polar angle of the recoil proton versus the polar angle of the scattered $K$ meson in the laboratory system, at an incident momentum of 820 MeV/$c$. The approximate acceptance band for elastic events used in this experiment is also shown, and is wider at the extremes to allow for multiple scattering.

differences between the duplicate measurements of projected angles form an approximately Gaussian distribution with a half-width of $\pm 0.4°$. A similar distribution in the measured separation of the two images of the sparks gives a half-width corresponding to $\pm 0.7$ cm in the height of each spark. These values were used in estimating the errors in the polar scattering angles for each event, which enter into the kinematic fit. The propagation of errors in the extrapolation back to the vertex along the two outgoing tracks allows the determination of the height of the vertex to only $\pm 1.7$ cm.

The frequency of gross mismeasurements (for example, the misreading of the angular scale by 10°) was estimated by a comparison of the rough measurements of the projected angles made by the authors with the corresponding results of the scanners. When limited to fiducial events, such mismeasurements do not eliminate more than 2–3% of good events and introduce a negligible number of background events into the acceptance bands.

The fiducial region was chosen to avoid events from the stainless steel walls of the target cell, and to avoid regions of the hydrogen cell for which the detection efficiency was small. The region chosen was a rectangular parallelepiped 8.0 cm long along the beam direction, 4.5 cm wide, and 7.0 cm in height. In addition, only events were accepted for which the azimuthal angle $\phi$ was between $\pm 35.0$ deg. With this choice of fiducial region, the weights applied to the individual events varied between 1.09 and 4.0, with very few greater than 2.5.

### D. Fit to Kinematics

A plot of the polar angle of the recoil proton versus the polar scattering angle of the $K$ meson is given in Fig. 6. The approximate acceptance bands for elastic events are indicated in the figure, and are wider at the extreme angles to allow for greater multiple scattering there.

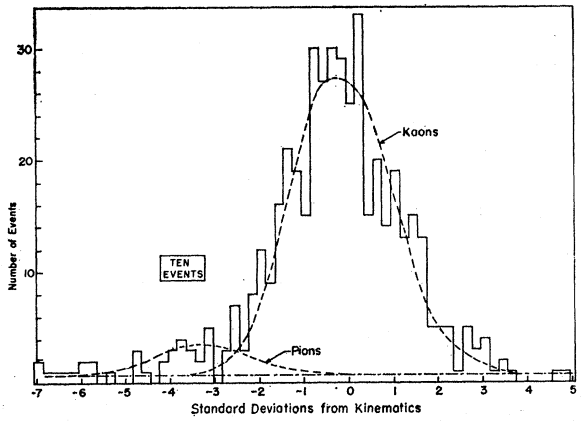


FIG. 7. The distribution of backscattered events in the number of standard deviations from the $K$ kinematics at 1040 MeV/$c$. Pion scattering events show in this distribution as a secondary peak at $-3.5$ standard deviations. (See Fig. 8.)

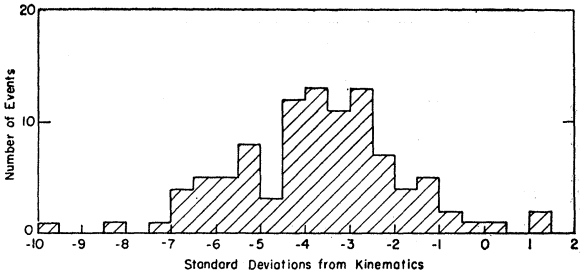


FIG. 8. The distribution of backscattered events from a sample of pion scatterings in the number of standard deviations in angle from $K$ kinematics. This sample was taken at 1040 MeV/$c$ by running the equipment with the Čerenkov counter removed from the trigger logic.

Each observed event is represented on this plot by two points, one for each choice of proton track. Error ellipses were constructed centered on the measured angles, with eccentricity set by the ratio of the estimated errors in the angles. The best estimate of the "true" scattering angles and the center-of-mass scattering angle $\theta^*$ was taken from the point of contact of the ellipse which was tangent to the nearest branch of the kinematic curve. The size of this ellipse in units of the estimated errors was taken as the number of standard deviations of the event from the kinematics. The errors in the angles due to multiple scattering between the origin of the event and the visible portion of the chamber were calculated and folded in with the measurement errors.

A distribution of the number of events as a function of number of standard deviations in angle from the kinematics is shown in Fig. 7 for backscattered events. The width of the distribution was found to be independent of $\cos\theta^*$, indicating that the error estimates were reasonable. Events were accepted as elastic out to $\pm 2.5$ standard deviations.

Pion events should appear in this distribution as a secondary peak at $-3.5$ standard deviations. This was verified in the analysis of a sample of 4000 photographs of pion events at 1040 MeV/$c$, taken by running the experiment with the Čerenkov output removed from the trigger logic. The distribution of backscattered pions when analyzed as kaons is shown in Fig. 8. The size of this secondary peak was used to cross check the pion contamination as estimated from the Čerenkov response curves (see Sec. III F).

Figure 9 shows a distribution of all events at 1040 MeV/$c$ versus the coplanarity parameter. The distribution has its peak near zero volume, as expected for elastic scattering of beam particles. Events were accepted as coplanar when the volume for the individual events was less than 0.16 in magnitude. The average of the estimates of the error in this volume for the indi-

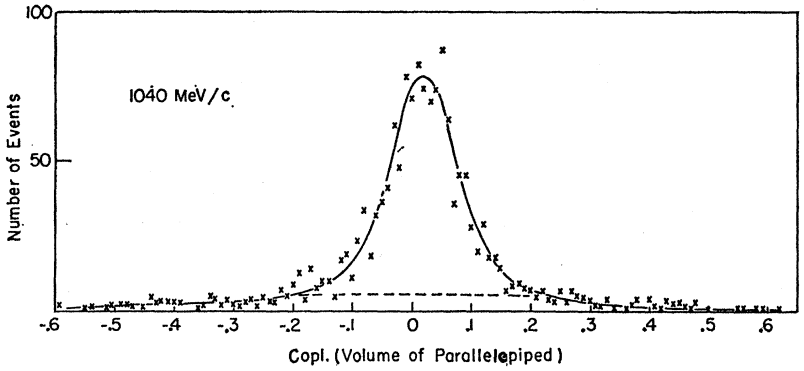


FIG. 9. The distribution of events in coplanarity for the 1040-MeV/$c$ data. The coplanarity criterion used is the volume of the parallelepiped which has three of its unit sides along the incident and outgoing track directions.

vidual events was $\pm 0.055$, consistent with the observed width of the distribution.

### E. Corrections for Losses of Events

Events were lost if the secondary particles failed to provide either the appropriate signature in the trigger counters or a visible set of sparks in the chamber along the correct direction. Such losses could have been due to a malfunction of the spark chamber or triggering system, to the geometry of particular events, or to the decay or interaction of the secondary particles.

The response of the cylindrical trigger counters in the median plane was studied as a function of their orientation by rotating the entire hydrogen target assembly about its axis in a well-defined 1-BeV/$c$ pion beam. The measured efficiencies were found to be greater than 98%, and independent of orientation.

No evidence for any systematic variation in the spark-chamber response was found in the geometric distribution of observed events, and an earlier measurement of $\pi^- - p$ elastic scattering angular distributions at[13] 868 MeV with the same spark chamber but a different triggering system gave good agreement with other measurements.[14]

The corrections for geometric effects were small except in the extreme $\cos\theta^*$ bins. There the projected angle of one of the tracks is small, and events were lost, for example, if one particle left the spark chamber through the beam channel (see Fig. 2 and Sec. II C). In many cases these missed events would have been seen from the same origin if the forward track had gone to the opposite side of the beam. To correct for loss of events at these angles, observed events were tabulated in the angular distributions with a relative weight of two if their hypothetical mirror events with the same origin and projected angles, but with the right and left tracks interchanged, could not be detected.

Correction was made similarly for the loss of events within the $\pm 35°$ range accepted in azimuth in which a high or low position in the target resulted in one particle missing the top or bottom of the trigger counters and/or plates. This was done by consideration of the mirror events obtained by inverting the sign of the dip angles of the tracks, both before and after the right-left interchange. The maximum possible weight for an individual event then became four.

Some events were lost because they occurred in certain portions of the target in which they could not be detected in any of the above four permutations. Correction was made for this loss by multiplying the weight of observed events with similar angles originating in an observable portion of the target by the ratio of the total length of the fiducial region along the beam to the corresponding length of the observable portion.

To limit the fluctuations in the assigned weights due to measurement errors, the mean weight and the deviation from the mean were calculated with the angles and vertex coordinates varied about their measured values according to a Gaussian distribution with width set by the estimated errors. The cutoffs chosen for the events included in the angular distributions were such that few events had a weight larger than 2.5. The largest correction was applied to the most backscattered bin in each angular distribution, where the average weight was 1.7. The most forward bins had an average weight of 1.1.

Correction was made for events lost by decay and interaction by multiplying the event weight by the inverse of the probability that one or both particles do not survive past the first set of gaps. For the range of energies in this experiment this correction varied between 1.09 and 1.35, depending on the dip angle through the materials as well as on $\cos\theta^*$.

### F. Estimation of Backgrounds

The contribution of inelastic processes to the fiducial sample of events was of the order of 8% of the total. It was estimated by linear extrapolation from the wings of two distributions: that of the number of events with acceptable coplanarity versus deviations from the

[13] M. A. Wahlig, Ph.D. thesis, Massachusetts Institute of Technology, 1962 (unpublished); and M. A. Wahlig, P. M. Fishbane, D. H. Frisch, W. Gerace, I. Mannelli, and L. Sodickson (to be published).

[14] B. J. Moyer, Rev. Mod. Phys. 33, 367 (1961).

kinematics (e.g., Fig. 7), and of kinematically acceptable events versus the coplanarity parameter (e.g., Fig. 9). An average of the two extrapolations was taken for each $\cos\theta^*$ bin, on the assumption that there is no correlation between the distance from the kinematics and the coplanarity parameter for the inelastic processes.

The contribution of pion events accepted in each $\cos\theta_K^*$ bin was obtained from the estimated pion flux, the published pion differential cross sections,[14] and the probability that a pion event be accepted as a $K$ elastic scattering.

The accepted pion flux was taken as the upper limit estimated from the kaon flux and the measured peak to valley ratio in the Čerenkov counter response curves. This number ranged between 1.6 and 4% of the number of $K$'s at the Čerenkov counter.

The probability that a pion event be accepted as an elastic scattering of a $K$ was estimated as a function of $\cos\theta_K^*$ (and $\cos\theta_\pi^*$) by considering the overlap with the $K$ acceptance band of a Gaussian distribution of events centered on the pion kinematics with a width set by the measurement and multiple scattering errors. Figure 10 shows this estimate at 820 MeV/$c$.

The pion contamination obtained in this way checked well with an estimate made from the size of the pion peak in the distribution of number of events versus deviations in angle from the kinematics, for the back-scattered $K$ region (e.g., Fig. 7). The number of pion events subtracted from the data was roughly 2% of the total number of elastic events.

The number of events exchanged between the forward and reversed elastic bands was estimated in a similar way by considering the overlap of a Gaussian distribution of events about one branch with the acceptance band of the other. The maximum number of events so exchanged occurred between the two bins nearest the crossing point, and corresponded roughly to 25% of the difference between the observed number of events in those bins. The correction amounts typically to an exchange of 1 or 2 events out of the 30 seen in each bin.

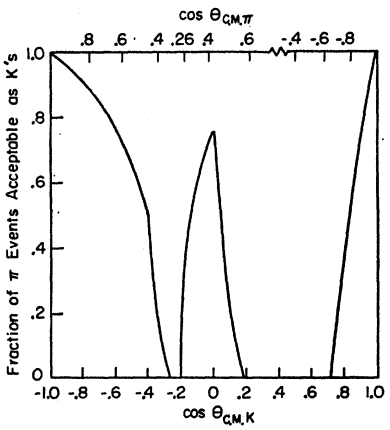


FIG. 10. The estimated fraction of pion elastic-scattering events which fall within the acceptance band about the $K$ kinematics, as a function of the cosine of the $K$ (and $\pi$) c.m. scattering angle.

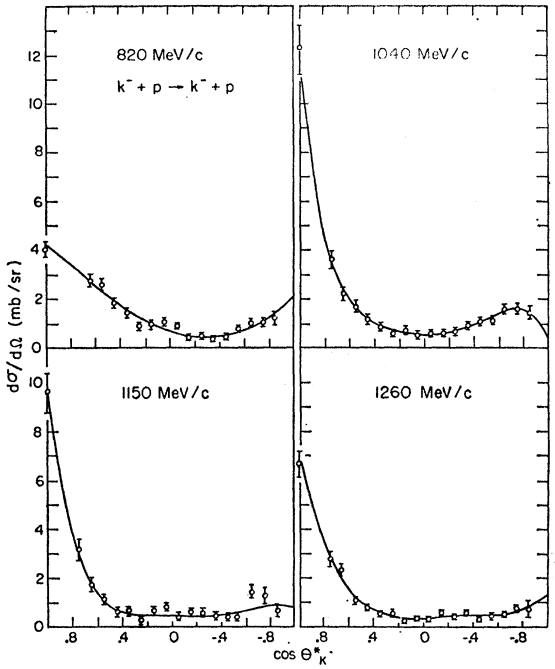


FIG. 11. The differential elastic-scattering cross sections for $K^-+p \to K^-+p$ as a function of the cosine of the $K$ c.m. scattering angle. The points at $\cos\theta^*=1.0$ represent the square of the imaginary part of the forward scattering amplitude as calculated from the total cross section by means of the optical theorem. An 8% error was assumed for these points to allow for uncertainties in normalization. The error bars on the other points represent both the statistical and the estimated internal systematic errors. The curves shown represent the best least-square fit of the data to a series in $\cos^n\theta^*$, and are the third-order fit at 820, fifth order at 1040 and 1150, and fourth order at 1260 MeV/$c$.

## G. Normalization

The primary normalization of the differential cross section was obtained from the monitored number of $K$ mesons incident on the target during each experimental run. This number was corrected for the decay of $K$ mesons in the region between the Čerenkov counter and the hydrogen target; the fraction which decayed varied between 10% and 15% for the different momenta.

Further corrections were made for the percentage of the beam discarded in the selection of the fiducial region (4%), the cuts in coplanarity and deviations from the kinematics (2%) (as estimated by graphical integration of the appropriate distributions), for scanning or measurement errors (5%), and for the pion contamination in the beam at the hydrogen target (3%).

The decay and interaction of the incident beam of $K$ mesons in the hydrogen target itself produced a slight decrease in the beam flux across the length of the target. This amounted to a 1% effective depletion in the worst case.

The final results are then as follows: 1 mb/sr corresponded to 57, 50, 22, and 52 events per 0.1 $\cos\theta^*$ bin at 820, 1040, 1150, and 1260 MeV/$c$, respectively. An

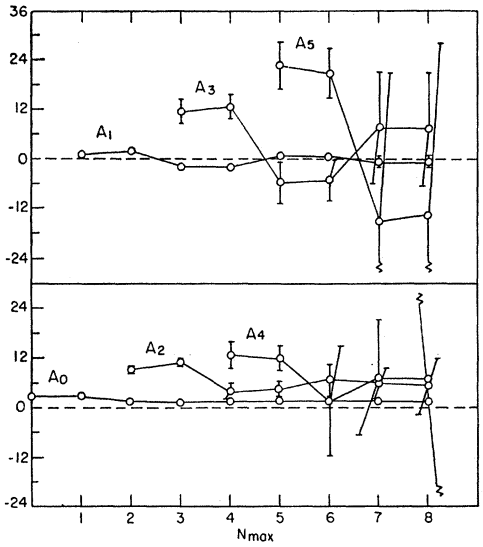


FIG. 12. A plot of the $\cos^n\theta^*$ expansion coefficients $A_n$ for the 1040-MeV/$c$ data as a function of the order of the fit. It should be noted that in general there is a strong variation of a coefficient $A_k$ when the order of the fit is equal to $k+2$. This effect persists even after the order of the fit has reached its optimum value ($N_{\max}=5$ in this case) according to the standard $\chi^2$ test.

error of 8% was assumed for each of these figures to allow for systematic errors in the estimations quoted above, and for possible errors in the calibration of the stereo system and hence the effective solid angle of the detector.

TABLE I. Differential elastic scattering[a] cross section for $K^-+p\rightarrow K^-+p$ in mb/sr.

| $P$(MeV/$c$) $\cos\theta^*$ | 820 | 1040 | 1150 | 1260 |
|---|---|---|---|---|
| 1.00 | 4.0 ±0.32 | 12.2 ±0.98 | 9.60±0.79 | 6.70±0.54 |
| 0.76 | | | | 2.80±0.30 |
| 0.75 | | 3.59±0.33 | 3.19±0.48 | |
| 0.65 | | 2.17±0.24 | 1.75±0.34 | 2.38±0.23 |
| 0.64 | 2.74±0.25 | | | |
| 0.55 | 2.59±0.24 | 1.72±0.21 | 1.16±0.28 | 1.08±0.17 |
| 0.45 | 1.82±0.20 | 1.16±0.17 | 0.60±0.20 | 0.80±0.15 |
| 0.35 | 1.46±0.17 | 0.88±0.16 | 0.65±0.21 | 0.56±0.13 |
| 0.25 | 0.88±0.14 | 0.59±0.13 | 0.25±0.15 | 0.57±0.13 |
| 0.15 | 0.94±0.14 | 0.71±0.14 | 0.65±0.21 | 0.24±0.10 |
| 0.05 | 1.08±0.16 | 0.53±0.11 | 0.77±0.23 | 0.31±0.10 |
| −0.05 | 0.86±0.15 | 0.60±0.12 | 0.40±0.17 | 0.30±0.10 |
| −0.15 | 0.43±0.10 | 0.62±0.12 | 0.56±0.19 | 0.58±0.12 |
| −0.25 | 0.47±0.11 | 0.65±0.13 | 0.56±0.19 | 0.43±0.10 |
| −0.35 | 0.38±0.06 | 0.88±0.15 | 0.41±0.16 | 0.54±0.12 |
| −0.45 | 0.45±0.10 | 1.02±0.17 | 0.33±0.16 | 0.31±0.09 |
| −0.55 | 0.77±0.14 | 1.08±0.17 | 0.39±0.17 | 0.45±0.11 |
| −0.65 | 0.98±0.16 | 1.54±0.21 | 1.44±0.30 | 0.52±0.12 |
| −0.75 | 1.02±0.17 | 1.55±0.23 | 1.24±0.30 | 0.77±0.16 |
| −0.85 | 1.17±0.31 | 1.41±0.27 | 0.59±0.28 | 0.66±0.31 |

[a] The values used at $\cos\theta^*=1.0$ represent the imaginary part of the forward scattering amplitude as calculated from the total cross section data of Ref. 6 with the optical theorem. The error used at $\cos\theta^*=1.0$ is the 8% uncertainty in absolute normalization, which is independent of incident momentum. The errors for the other points represent just the statistical and internal systematic errors, and do not include the uncertainty in absolute cross section.

## IV. EXPERIMENTAL RESULTS

Figure 11 shows the differential cross sections obtained at 820, 1040, 1150, 1260 MeV/$c$, respectively. The measured cross sections are given in Table I. The point at $\cos\theta^*=1.0$ at each energy was evaluated solely from the total cross sections[6] by means of the optical theorem assuming the forward scattering amplitude to be entirely imaginary; thus this point is only a lower limit to the differential cross section at 0°. An 8% error was assumed for these points at zero degrees to allow for the uncertainty in normalization.

The data were fitted with a power series expansion in $X=\cos\theta^*$ of the form

$$d\sigma/d\Omega=(\lambda\!\!\!^{-2}/4)\sum_{n=0}^{N\max}A_nX^n. \tag{1}$$

To aid in the determination of the correct order of fit, i.e., the highest value of $N_{\max}$ required, the data were also analyzed in a series of Legendre polynomials of the form

$$d\sigma/d\Omega=(\lambda\!\!\!^{-2}/4)\sum_{n=0}^{N\max}B_nP_n(X). \tag{2}$$

The fitted curve, of course, is the same since the leading term in $P_n(X)$ is $X^n$. The $P_n(X)$ have the advantage of forming an orthogonal set, and therefore, when the difference between the fitted curves of successive order becomes small, the $B_n$ do not change appreciably as higher terms are added, while the $A_n$ do. As an example,

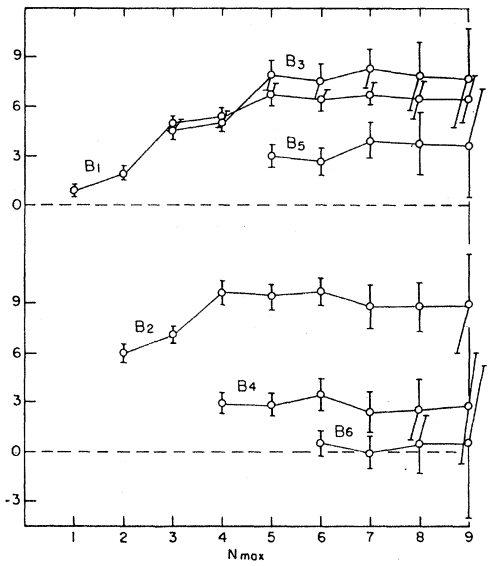


FIG. 13. A plot of the Legendre polynomial expansion coefficients $B_n$ for the 1040-MeV/$c$ data as a function of the order of the fit. As expected from the orthogonality of the Legendre polynomials, there is no appreciable change in a coefficient $B_k$ once $N_{\max}$ has reached its optimum value ($N_{\max}=5$ in this case) according to the standard $\chi^2$ test.

TABLE II. $K^-$–$p$ differential elastic-scattering cross section fitted to $d\sigma/d\Omega = (\chi^2/4)\,\Sigma\, A_n \cos^n\theta^*$.

| $P$ (MeV/$c$) | Order of fit | $A_0$ | $A_1$ | $A_2$ | $A_3$ | $A_4$ | $A_5$ | $A_6$ | $A_7$ | $(\chi^2/f)^{1/2}$ | Integral |
|---|---|---|---|---|---|---|---|---|---|---|---|
| 820 | 2 | 1.39±0.10 | 2.94±0.20 | 5.11±0.41 | | | | | | 1.28 | 18.5±0.7 |
| | 3 | 1.42±0.10 | 3.39±0.34 | 5.12±0.41 | −1.19± 0.71 | | | | | 1.24 | 18.7±0.7 |
| | 4 | 1.38±0.13 | 3.38±0.34 | 5.89±1.17 | −0.99± 0.77 | −1.09± 3.57 | | | | 1.28 | 18.6±0.7 |
| | 5 | 1.36±0.13 | 3.23±0.57 | 5.84±1.18 | 0.12± 3.33 | −0.81± 1.76 | −1.22± 3.56 | | | 1.33 | 18.8±0.9 |
| 1040 | 3 | 1.39±0.15 | −1.82±0.60 | 11.1 ±0.71 | 11.4 ± 1.49 | | | | | 1.65 | 21.3±0.8 |
| | 4 | 1.77±0.18 | −2.09±0.60 | 3.95±1.82 | 12.6 ± 1.52 | 12.8 ± 3.00 | | | | 1.24 | 23.6±1.0 |
| | 5 | 1.74±0.17 | 0.51±0.90 | 4.39±1.82 | −5.78± 4.94 | 11.8 ± 3.00 | 22.5 ± 5.78 | | | 0.63 | 23.3±1.0 |
| | 6 | 1.67±0.20 | 0.41±0.91 | 6.77±3.67 | −4.76± 5.13 | 2.05±13.4 | 20.8 ± 6.21 | 9.03±12.1 | | 0.62 | 23.6±1.0 |
| | 7 | 1.69±0.20 | −0.53±1.30 | 5.91±3.77 | 7.65±13.3 | 7.10±14.3 | −15.5 ±36.5 | 2.29±13.8 | 28.0±27.7 | 0.56 | 22.6±1.4 |
| 1150 | 3 | 0.75±0.24 | −1.51±0.79 | 10.4 ±1.05 | 12.8 ± 1.92 | | | | | 1.95 | 15.4±1.0 |
| | 4 | 1.66±0.29 | −1.98±0.79 | −2.26±2.56 | 13.7 ± 1.93 | 20.2 ± 3.73 | | | | 1.35 | 18.0±1.1 |
| | 5 | 1.62±0.29 | 0.44±1.32 | −1.62±2.58 | −2.05± 7.15 | 18.3 ± 3.82 | 17.5 ± 7.66 | | | 1.25 | 17.3±1.1 |
| | 6 | 2.06±0.30 | 0.95±1.34 | −13.2 ±5.60 | −7.30± 7.50 | 64.5 ±20.1 | 26.8 ± 8.61 | −41.2 ±17.5 | | 1.09 | 17.0±1.2 |
| | 7 | 2.08±0.30 | −1.77±2.01 | −14.4 ±5.62 | 26.2 ±20.0 | 74.3 ±20.8 | −70.1 ±54.0 | −56.6 ±19.5 | 73.5±40.0 | 0.99 | 14.8±1.7 |
| 1260 | 3 | 0.96±0.16 | −0.49±0.61 | 9.85±0.74 | 11.7 ± 1.52 | | | | | 1.49 | 13.6±0.6 |
| | 4 | 1.36±0.19 | −0.62±0.61 | 3.24±1.82 | 11.4 ± 1.52 | 11.5 ± 2.90 | | | | 1.10 | 15.2±0.7 |
| | 5 | 1.37±0.19 | −1.20±0.96 | 2.99±1.85 | 15.3 ± 5.20 | 12.3 ± 3.08 | −4.61± 5.89 | | | 1.12 | 15.5±0.8 |
| | 6 | 1.41±0.22 | −1.17±0.97 | 1.75±3.79 | 14.7 ± 5.39 | 17.3 ±13.8 | −3.49± 6.61 | −4.69±12.5 | | 1.16 | 15.4±0.9 |

Figs. 12 and 13 show the behavior of the $A_n$ and $B_n$ as a function of $N_{\max}$, at 1040 MeV/$c$.

In selecting the best fit, it was required that the goodness of fit parameter $(\chi^2/f)^{1/2}$ be at or near its minimum value and that the $B_n$ be stable as functions of $N_{\max}$. The fitted curves with and without the optical theorem points were required to agree reasonably well. The fitted curves were required not to exhibit nonphysical behavior, in the sense that the differential cross section must be everywhere positive, and have positive slope at $X=1.0$.

With these criteria, a third-order fit at 820, fifth order at 1040, and fourth order at 1260 MeV/$c$ are necessary and sufficient to fit the data.

The 1150-MeV/$c$ data, for which we obtained only half as many events as at the other energies, are adequately fitted by a fifth-order polynomial on the basis of the goodness of fit parameter, with sixth order slightly better. However, when fitted to the data without the optical theorem point as constraint, the sixth-order curve becomes negative for $\cos\theta^* < -0.9$, and turns down to 2.5 mb/sr at $X=1.0$ whereas the fifth-order fit is nearly the same with and without the point at 0°. Within the poor statistics for this point we conclude that the fifth-order fit is best, and that the behavior of the sixth- and higher-order curves are due to fluctuations in the measured cross sections at $X=-0.65$ and $-0.75$.

The total elastic cross sections obtained by integration of the selected curves are shown in the upper curve in Fig. 14 with the results of other experiments for comparison. The charge exchange cross section is also shown. The errors shown for our points do not include the 8% uncertainty assumed for the absolute normalization. (This uncertainty is essentially geometric and independent of the energy.) The agreement with the other experiments is in general good. It should be noted that the points of Beall *et al.*[15] represent a preliminary sample of their data and have had few corrections applied. Final corrections for the entire sample are still in progress.[16]

The values of some of the $A_n$ and $B_n$ coefficients and their errors in Eq. (1) are given in Tables II and III for the different momenta. The coefficients of the third-order fit at 820, fifth order at 1040 and 1150, and fourth

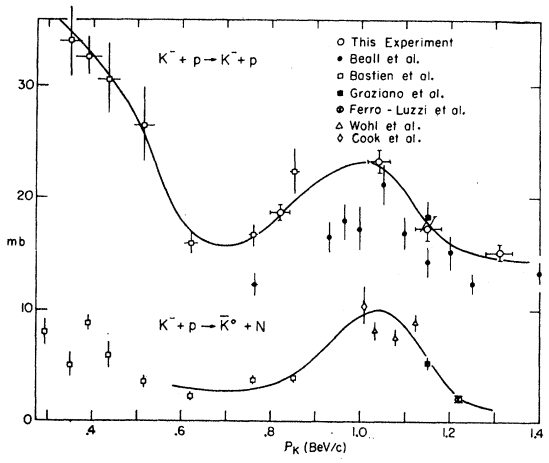


FIG. 14. A plot of the total $K^-$ proton elastic scattering and elastic charge exchange cross sections as a function of bombarding momentum. The values shown for our points were obtained by integration of the third-order fit at 820, fifth order at 1040 and 1150, and fourth order at 1260 MeV/$c$. The errors shown for each point represent both the statistical and systematic errors, with the exception of an 8% uncertainty in the absolute normalization which is the same for all four points. The horizontal bars represent the ±2.5% momentum resolution.

[15] E. F. Beall, W. Holley, D. Keefe, L. T. Kerth, J. J. Thresher, C. L. Wang, and W. A. Wenzel, in *Proceedings of the 1962 International Conference on High-Energy Nuclear Physics at CERN* (CERN, Geneva, 1962), p. 368.

[16] D. Keefe (private communication).

TABLE III. $K^-$–$p$ differential elastic-scattering cross section fitted to $d\sigma/d\Omega = (\lambda^2/4)\sum B_n P_n(\cos\theta^*)$.

| $P$ (MeV/$c$) | Order of fit | $B_0$ | $B_1$ | $B_2$ | $B_3$ | $B_4$ | $B_5$ | $B_6$ | $B_7$ |
|---|---|---|---|---|---|---|---|---|---|
| 820 | 2 | 3.09±0.11 | 2.94±0.20 | 3.40±0.27 | | | | | |
| | 3 | 3.13±0.11 | 2.68±0.25 | 3.41±0.27 | −0.477±0.28 | | | | |
| | 4 | 3.11±0.12 | 2.79±0.30 | 3.31±0.31 | −0.39 ±0.31 | −0.25±0.35 | | | |
| | 5 | 3.15±0.16 | 2.78±0.31 | 3.43±0.49 | −0.49 ±0.42 | −0.18±0.40 | −0.16±0.45 | | |
| 1040 | 3 | 5.08±0.18 | 5.02±0.50 | 7.37±0.48 | 4.56 ±0.60 | | | | |
| | 4 | 5.64±0.23 | 5.46±0.51 | 9.93±0.77 | 5.03 ±0.60 | 2.92±0.69 | | | |
| | 5 | 5.57±0.23 | 6.70±0.61 | 9.61±0.77 | 7.70 ±0.92 | 2.70±0.69 | 2.86±0.73 | | |
| | 6 | 5.63±0.24 | 6.47±0.68 | 9.99±0.88 | 7.35 ±1.03 | 3.29±1.04 | 2.64±0.79 | 0.62±0.84 | |
| | 7 | 5.41±0.33 | 6.75±0.73 | 9.08±1.25 | 8.05 ±1.24 | 2.33±1.41 | 3.77±1.37 | 0.16±0.96 | 1.04±1.03 |
| 1150 | 3 | 4.23±0.26 | 6.18±0.68 | 6.95±0.70 | 5.13 ±0.76 | | | | |
| | 4 | 4.95±0.29 | 6.25±0.68 | 10.04±0.90 | 5.49 ±0.77 | 4.62±0.85 | | | |
| | 5 | 4.74±0.30 | 6.73±0.71 | 9.35±0.95 | 6.98 ±1.01 | 4.17±0.87 | 2.23±0.97 | | |
| | 6 | 4.66±0.31 | 8.04±0.90 | 8.43±1.03 | 8.97 ±1.32 | 1.92±1.30 | 3.40±1.09 | −2.85±1.21 | |
| | 7 | 4.05±0.45 | 8.42±0.93 | 5.91±1.72 | 10.52 ±1.57 | −0.66±1.93 | 6.17±1.88 | −3.92±1.35 | 2.74±1.51 |
| 1260 | 3 | 4.25±0.19 | 6.51±0.52 | 6.57±0.49 | 4.67 ±0.61 | | | | |
| | 4 | 4.74±0.22 | 6.21±0.53 | 8.73±0.74 | 4.55 ±0.61 | 2.63±0.66 | | | |
| | 5 | 4.83±0.25 | 5.98±0.60 | 9.02±0.83 | 4.06 ±0.87 | 2.81±0.71 | −0.58±0.75 | | |
| | 6 | 4.79±0.27 | 6.18±0.80 | 8.85±0.95 | 4.34 ±1.16 | 2.50±1.09 | −0.43±0.84 | −0.32±0.87 | |

order at 1260 MeV/$c$ are plotted in Fig. 15 as a function of bombarding momentum. The values shown for $A_4$ and $A_5$ at 820, and $A_5$ 1260 MeV/$c$, are from the fifth-order fits, and are included to give an estimate of their error.

## V. DISCUSSION OF RESULTS

In contrast to the analysis of the 395-MeV/$c$ $K^-$–$p$ resonance ($Y_0^*$ 1520 MeV, see Ferro-Luzzi *et al.*[4]) in which the behavior of the $A_n$ coefficients in the elastic scattering allowed a unique determination of the spin and parity of the resonant state, the analysis of the present data in terms of a single resonant state superimposed on a single background does not yield as conclusive a result. Some quantitative statements can nevertheless be made, following an analysis of the type used by Layson[17] in his study of the pion-nucleon scattering results.

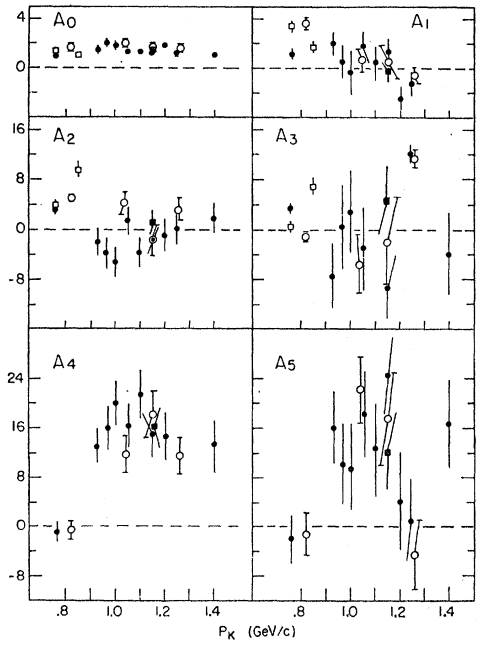


FIG. 15. A plot of the $\cos^n\theta^*$ coefficients $A_n(N_{max}=5)$ as a function of incident momentum. The symbols used are the same as those in Fig. 14. The values of $A_0$ through $A_3$ at 820, and $A_0$ through $A_4$ at 1260 MeV/$c$ are from the third- and fourth-order fits, respectively. All other values are from the respective fifth-order fits. The errors shown at the different momenta assume that the chosen fit is the correct order, and should of course be considered in conjunction with the respective values of $\chi^2$.

The integrated elastic scattering cross section shows an ~7-mb resonance with a maximum at approximately the same energy as the total cross section.[6] As expected from isotopic symmetry, the results for the elastic charge exchange cross section[5,18–20] show a similar peak of approximately the same height (see Fig. 14). The two together account for almost all of the resonance in the total cross section, indicating that the resonant state is largely elastic.

The fact that the $A_4$ and $A_5$ coefficients are quite different from zero for momenta higher than ~850 MeV/$c$ indicates the presence of $J=5/2$ states, and confirms the hypothesis made on the basis of the size of the resonant part of the total cross section[6,21] that the spin of the resonant state is at least equal to 3/2. On the other hand, the absence of a significant $A_6$ coefficient below 1260 MeV/$c$ indicates that angular momentum states with $J$ greater than 5/2 do not dominate the elastic scattering in the resonance region. It should be

[17] W. M. Layson, Nuovo Cimento **27**, 724 (1963).
[18] P. L. Bastien, J. P. Berge, O. I. Dahl, M. Ferro-Luzzi, J. Kirz, D. H. Miller, J. J. Murray, A. H. Rosenfeld, R. D. Tripp, and M. B. Watson, in *Proceedings of 1962 International Conference on High Energy Physics at CERN* (CERN, Geneva, 1962), p. 373; M. Ferro-Luzzi, F. T. Solmitz, and M. L. Stevenson, *ibid.*, p. 376.
[19] W. Graziano and S. O. Wojcicki, Phys. Rev. **128**, 1868 (1962).
[20] C. Wohl, M. H. Alston, G. R. Kalbfiesch, D. H. Miller, and S. O. Wojcicki, Bull. Am. Phys. Soc. **8**, 340 (1963), and (private communication).
[21] R. H. Dalitz, Brookhaven National Laboratory Report BNL 735 (T 264), December 1961, p. 32 (unpublished).

noted that with the present statistics our data do not extend far enough in the forward and backward scattering regions to be strongly sensitive to the presence of partial waves with $J$ much greater than 5/2. Using only waves with $J \leq 7/2$, we find that the simplest assignment for the spin of the resonance is $J=5/2$.

The large magnitude of $A_5$ and its change with bombarding momentum indicates the presence of both $D_{5/2}$ and $F_{5/2}$ states, with one or both of these amplitudes changing rapidly in the resonance region. The behavior of the $A_4$ coefficient does not yield significant additional information about the parity of the resonance because the $D_{5/2}$ and $F_{5/2}$ amplitudes contribute to its expansion in terms of partial wave in a nearly symmetric way, and the interpretation is complicated by the possible presence of $D_{3/2}$ and $P_{3/2}$ waves. The usefulness of the lower coefficients is limited because the number of amplitudes contributing to them is very large. Thus it is not possible to reach a definite conclusion as to the parity of the resonant state.

Ball and Frazer[22] predicted a $D_{3/2}$ resonance at this energy as a consequence of the strong production of the $K^*$ mesons near the $K^*$ threshold ($p_K \sim 1070$ MeV/$c$). This possibility cannot be excluded on the basis of the present data, since a very strongly elastic $D_{3/2}$ amplitude can give the observed behavior of $A_4$ and $A_5$ by interference with small $D_{5/2}$ and $F_{7/2}$ background amplitudes, respectively. The effects of these background amplitudes would not be large enough off resonance to be detected in the present experiment. Hence our only reason for favoring the $J=5/2$ assignment is the greater simplicity of the $D_{5/2}F_{5/2}$ interference model, in which only one background state is needed.

Barbaro-Galtieri *et al.*[23] found a new $K^-$-$p$ enhancement at a mass of 1765 MeV (corresponding to $\sim$930 MeV/$c$ in our experiment) in the analysis of the reaction $K^-+n \to K^-+\pi^-+p$ in the LRL 72-in. bubble chamber filled with deuterium. Stimulated by this discovery, they have analyzed the available elastic-scattering data[5,15,24] in terms of two adjacent resonances. They obtain reasonable agreement with the energy variation of the $A_4$ and $A_5$ coefficients as well as the total cross section by assuming a $D_{5/2}$ resonance at 1765 MeV and an $F_{5/2}$ resonance at 1815 MeV.

In summary, we feel that our present data alone do not warrant any more sophisticated interpretation than that of a single resonance in a $J=5/2$ wave, in interference with a strong background of the opposite parity $J=5/2$ wave, and other waves with $J<5/2$. No conclusion can be drawn concerning the parity of the resonant state.

## ACKNOWLEDGMENTS

The authors are greatly indebted to Dr. M. H. Blewett and the staff and floor crew of the Brookhaven A.G.S. for their cooperation and interest. The authors wish to express their thanks to Professor James H. Smith for his invaluable advice and assistance during the experimental runs.

Paul M. Mockett and Andrew Buffington were instrumental in the design, construction, and testing of the trigger and Čerenkov counters, and they and Robert O'Donnell, Stephen Smith, Stephen Pollock, and Jose Perez-Esandi gave freely of their time to help during the runs. The assistance of Eva Bonis in the analysis of the data is gratefully acknowledged.

One of us (I.M.) wishes to acknowledge financial support from NATO and the hospitality received from the Laboratory for Nuclear Sciences of MIT and from the Brookhaven National Laboratory. Some of the equipment used in this experiment was purchased with the support of the Alfred P. Sloan Foundation.

The MIT Computation Center generously provided time for part of this work on their IBM 7090 computer.

[22] J. S. Ball and W. R. Frazer, Phys. Rev. Letters 7, 204 (1961). We wish to thank W. R. Frazer for very helpful comments.

[23] A. Barbaro-Galtieri, A. Hussian, and R. Tripp, Lawrence Radiation Laboratory Report UCRL 10885 (unpublished) and private communication.

[24] L. Sodickson, Ph.D. thesis, Massachusetts Institute of Technology, January 1963 (unpublished).